Experiments in Imaging Rupture Properties and Early Aftershocks of Large Earthquakes

Award 04HQGR0097

Peter M. Shearer
Institute of Geophysics and Planetary Physics
Scripps Institution of Oceanography
University of California, San Diego
La Jolla, CA 92093
858-534-2260 (phone), 858-534-5332 (fax)
pshearer@ucsd.edu

Key words: Seismology, Seismotectonics, Source Characteristics

Annual Progress Summary Report

Investigations Undertaken

In consultation with National Earthquake Information Center (NEIC) researchers, we are investigating practical methods to routinely detect and image very early aftershocks of large earthquakes. Our work so far has focused on the 22 December 2003 Mw 6.5 San Simeon earthquake. Our method uses a matched-filter technique to back-project energy to the source region in order to image finite-source effects and locate early aftershocks that may be hidden in the coda of the mainshock. Our goal is to develop a method that can be implemented in real time that provides approximate aftershock locations and can be used to quickly identify the primary fault plane and the rupture propagation direction, information that can improve the rapid calculation of strong ground-motion predictions.

Results

Detection and Location of Early Aftershocks

Earthquake aftershocks provide one of the best ways to resolve the mainshock rupture plane. Aftershock occurrence rates are observed to decay with time and the highest rates are observed immediately following the mainshock. However, detection and location of these events are hampered by the mainshock coda and the difficulty in sorting out which seismic arrivals are coming from which event when multiple aftershocks occur at nearly the same time.

Automatic event detection and location schemes provide a possible way to locate many of these "missing" events. However, the presence of multiple events occurring at overlapping times complicates the task of constructing reliable algorithms for this purpose. An approach that may prove reliable under such circumstances is to construct a matched filter, based on predicted or empirical images of the arrival pattern from known events, to search for patterns in the data that suggest the occurrence of an earthquake. This approach has been successfully applied to continuous global seismic data to detect previously unidentified events (Shearer, 1994). The matched filter algorithm works as illustrated in Figure 1.

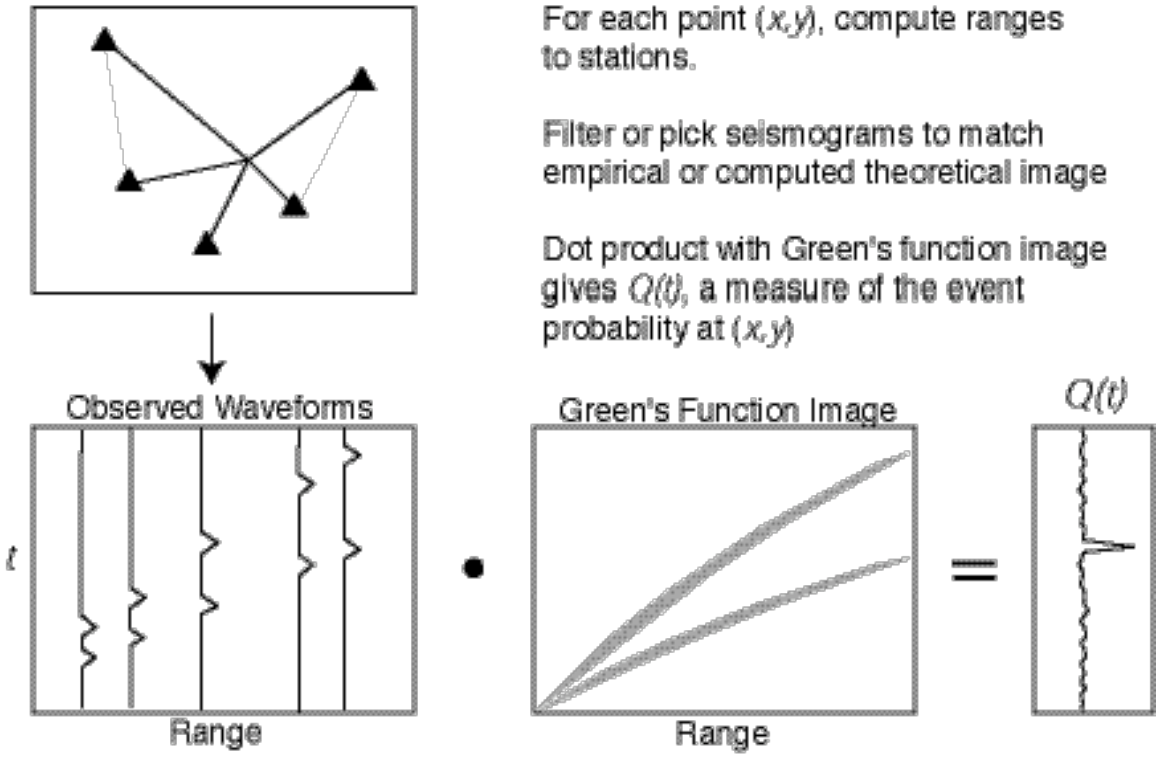

Figure 1. A cartoon illustrating the matched filter event detection and location method.

Assume we have seismograms $a_i(t)$ at stations $\mathbf{s}_i = (s_x, s_y)_i$. We run the seismograms through a processing filter $P[a_i(t)]$. This is any arbitrary function, i.e., a picking algorithm, automatic-gain-control filter, etc. We then use a series of records or synthetic seismograms from distributed events, $\mathbf{e}_j = (e_x, e_y, e_z, e_t)_j$, calculate the source-receiver ranges Δ_{ij}, and compute the Green's function image (matched filter) as

$$\mathbf{S}(\Delta_{ij}, T, e_z) = B\{P[a_i(t)], \mathbf{e}_j\}$$

where T is the time from the event origin time, and B is a stacking or processing method. For example, B might simply be an average of $P[a_i(t)]$ computed for all seismograms with source-receiver ranges within a small interval around Δ. Alternatively, B might be a convolution of $P[a_i(t)]$ with a simple reference wavelet.

For a given candidate location $\mathbf{q} = (q_x, q_y, q_z)$ and the filtered seismograms $P[a_i(t)]$, we compute the relative probability Q as the dot product

$$\mathbf{S}(\Delta, T, e_z) \cdot B\{P[a_i(t)], \mathbf{q}\} = Q(t, \mathbf{q})$$

The relative probability $Q(t, \mathbf{q})$ will have maxima which define the origin time and location of likely events. The method requires the computation of $Q(t, \mathbf{q})$ at thousands of points on the Earth's surface where candidate events may have taken place and a range of possible source depths. However, the technique is computationally feasible since $P[a_i(t)]$ need only be computed once; the dot product must be computed multiple times but this is a fast computation that is suited for vectorization schemes. Additional efficiency can be achieved by adopting a relatively coarse spatial grid to identify probable events and then applying finer local grids to refine the locations.

This matched filtering scheme is completely general and can be applied to any target image. For example, $\mathbf{S}(\Delta, T, e_z)$ could be defined using synthetic seismograms based on a reference earth model or simply by using a travel time curve for a target seismic phase (with suitable weighting schemes the method could be designed to mimic standard location algorithms). By adjusting the sharpness of the B function, the method can be tuned to precisely locate events with good signal-to-noise ratios or to obtain approximate locations for poor signal-to-noise events.

Results for 2003 San Simeon Earthquake

The 22 December 2003 Mw 6.5 San Simeon earthquake occurred near the central California coast in a relatively sparsely instrumented region (see Figure 2). The rupture propagated unilaterally to the southeast from the epicenter, causing strong directivity effects so that damage was concentrated to the southeast. The worst damage occurred in Paso Robles where two people died as a result of a building collapse. The absence of stations near the rupture initially limited the accuracy of the automatically-produced CISN ShakeMap (Hardebeck et al., 2004). Imaging early aftershocks would therefore have been helpful for this event in quickly constraining the rupture direction and areas of likely strong shaking.

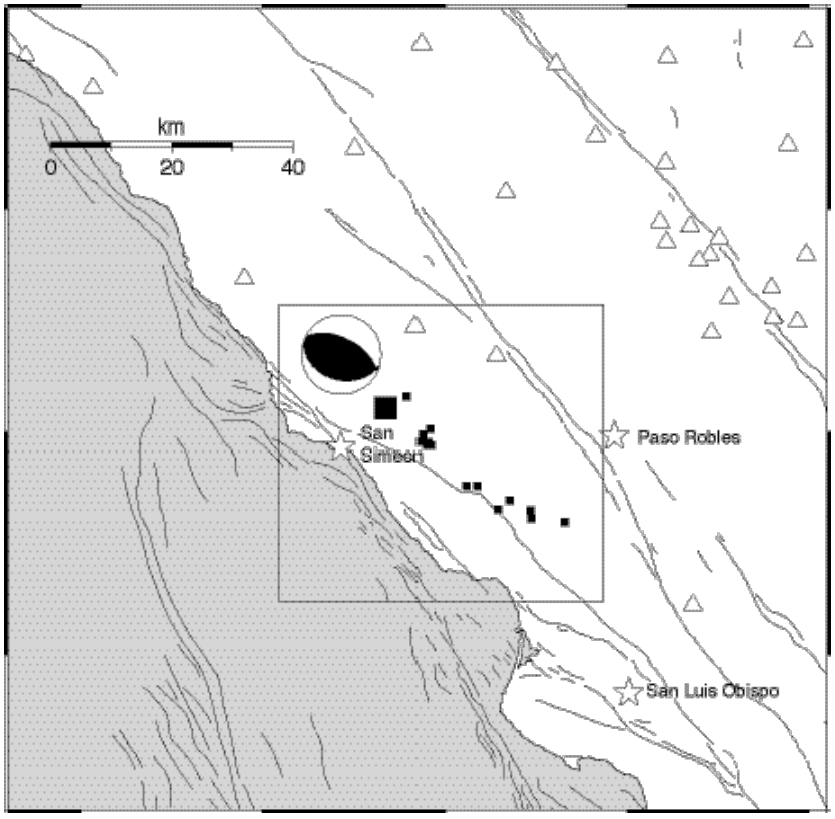

Figure 2. Map of the central California coast showing the epicenter of the December 22, 2003 M 6.5 San Simeon earthquake (large square). The NCSN-computed first-motion focal mechanism based on P polarities is also shown; moment tensor solutions give very similar results and indicate a reverse fault striking northwest-southeast. The rupture propagated unilaterally to the southeast. The small squares show the NCSN (Northern California Seismic Network) locations for aftershocks in the first 30 minutes following the mainshock. The triangles show locations of NCSN seismic stations. Thin lines delineate known fault traces (Jennings, 1975). The box shows the region plotted in Figure 4.

Due to the sparse instrument density in the region, and its proximity to the Pacific Ocean, most NCSN and CI stations that recorded waveforms are located to the northeast. This is an unfavorable source/station geometry, and consequently there is a tendency for the back-projected relative probability function (Q) to smear in the NE-SW direction given any scatter in the data. To determine the degree to which this geometry affects our method, we analyzed P phase picks from a test set of well recorded aftershocks before examining the more challenging time period of the first 30 minutes following the mainshock.

We implement the matched filter approach as follows:

(1) We define a grid of possible event locations at 700-m spacing in x/y and 1000-m spacing in depth, and compute P travel times from every grid point to every station.

(2) We convolve the pick distribution at each station with a Ricker wavelet of about 2-s period.

(3) Using the pre-computed travel times, we back-project the amplitudes along each trace to the appropriate position in the time series at each grid point. This summation defines the $Q(t, \mathbf{q})$ function.

(4) To estimate the times and locations of likely events, we perform a 4-D (x,y,z,t) gradient-checking grid search of $Q(t, \boldsymbol{q})$ to find all local maxima, and run this sequence of maxima through a filter that determines the maximum every 10 seconds.

Back-Projecting NCSN Associated Picks

We examined two post mainshock time windows of vertical-component waveforms for the 22 seismic stations. We first bandpass filtered the traces from 5 to 40 Hz and then applied the Earle and Shearer (1994) automatic picking algorithm. The resulting picks for the first 30 minutes are plotted in Figure 3, compared to the raw unassociated picks from the NCSN database. Both sets of picks indicate a significant number of aftershocks during this time period. However, the first 300 s of data recorded at many of the stations were plagued by waveform clipping (Figure 3), which makes picking aftershock phases in this period nearly impossible. Furthermore, filtering clipped data introduces spikes into the resulting waveforms that are then picked by the autopicker.

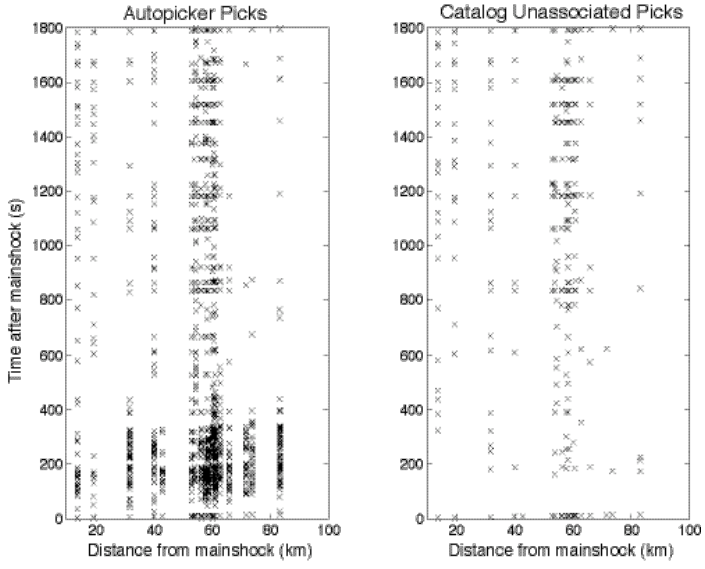

Figure 3. P-wave picks in the first 30 minutes following the San Simeon mainshock, as measured from the waveforms with the Earle and Shearer (1994) autopicker (left) and as obtained from the NCSN database (right).

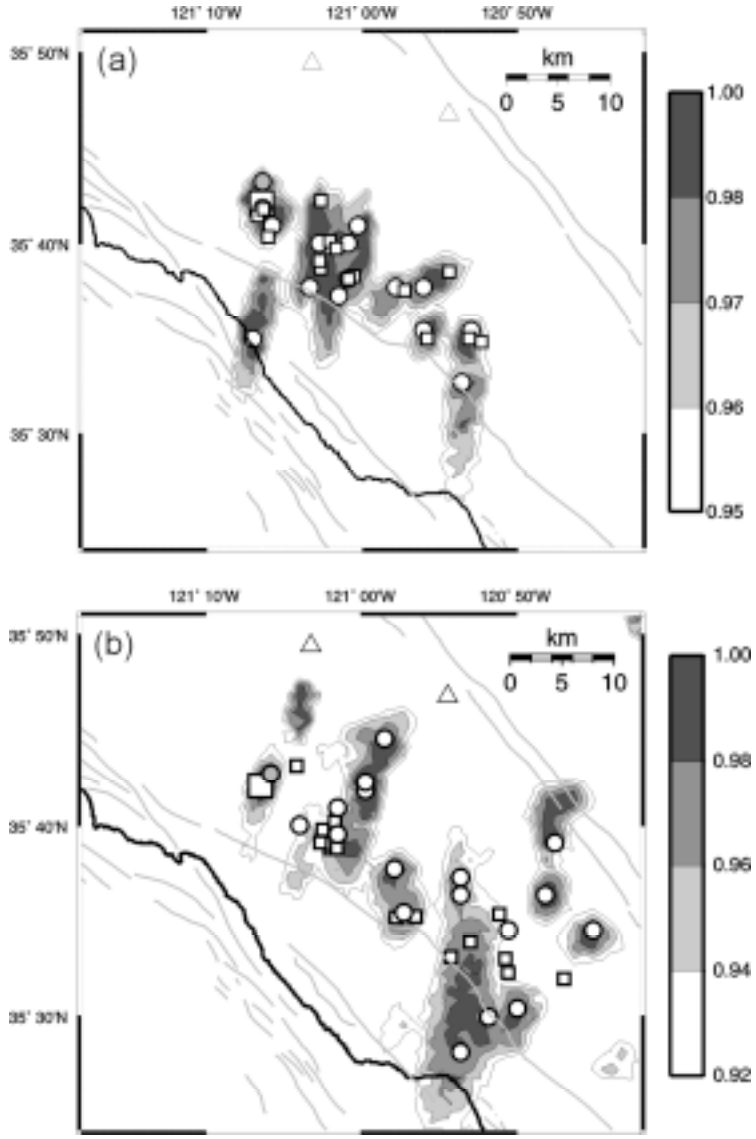

Figure 4. Results of San Simeon P phase picks back-projected in the region surrounding the rupture zone. Squares indicate NCSN event locations (large square: mainshock). Circles indicate detected event locations (gray mainshock, white aftershocks). Background shading is the relative probability of a detected event (Q). We back-projected (a) a hand-selected set of associated catalog picks that were identified at most stations during the first 3.5 hours post mainshock, and (b) picks from our autopicker that ran on data recorded on all stations in Figure 2 during the first 30 minutes post mainshock. NCSN locations in (a) were selected by hand to test the accuracy of the method. NCSN locations in (b) correspond to those in Figure 2.

Before attempting to backproject the autopicker results, we first tested how well the matched filter approach can image well-recorded aftershocks given the limited station coverage. We selected 16 events (including the mainshock) from the first 3.5 hours after the clipped zone for which picks were made at most of the 22 stations in Figure 2. We artificially adjusted these pick times so that the events occurred at ~2 minute intervals. For each 2-min period, we calculated the maximum Q at each grid point, and normalized this 2-D function by the maximum. After analyzing all events, we determined the maximum value of all 16 normalized surfaces at each grid point. The resulting event locations and normalized Q are

shown in Figure 4a. Although there is NNE/SSW smearing of $Q(t)$, all of the event locations are within 5 km of their associated NCSN aftershock locations (Figure 5), indicating that this technique is not compromised by a non-ideal station/source geometry. However, for picks made at only a handful of the 22 stations in Figure 2 (e.g., for the case of a small-magnitude aftershock), false relocations do occur that would not occur if the station geometry were more favorable. Preliminary tests of azimuth-weighting schemes to compensate for this difficulty have been promising, and suggests this challenge can be overcome.

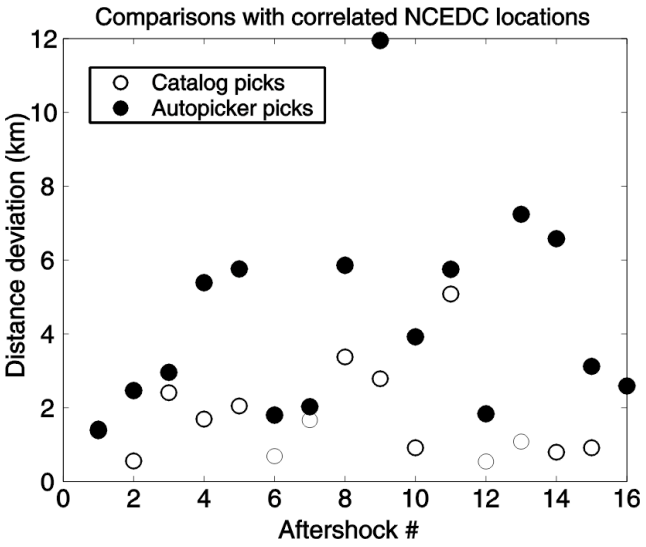

Figure 5. Comparison of aftershock locations using the NCSN catalog picks and picks from the Earle and Shearer (1994) autopicker. Aftershock # for each case corresponds to a different event.

Back-Projecting Autopicker Picks

The NCSN catalog contains 15 aftershocks (Figure 2) within the first 30 minutes after the mainshock. To determine if our method can resolve these as well as possible additional aftershocks during this time period, we similarly back-projected the picks from the autopicker (Figure 3), experimenting with different autopicking parameters. Our method successfully detected all 16 events and located all but one of them within 2.5 s and ~7 km of the associated NCSN catalog origin time/location (Figures 4b and 5). Furthermore, additional events with similar probabilities that are significantly separated in time (by several tens of seconds) from the other NCSN catalog events were detected. These events are most likely real aftershocks that have not been included in the NCSN catalog. Despite the erroneous picks from the filtered clipped waveforms, events were not falsely detected during the first 300 s following the mainshock. This is to be expected if there is an element of randomness in the onset and width of clipped waveforms at each station.

References

Earle, P.S. and P.M. Shearer, Characterization of global seismograms using an automatic picking algorithm, *Bull. Seismol. Soc. Am.*, **84**, 366–376, 1994.

Hardebeck, J.L., J. Boatwright, D. Dreger, R. Goel, V. Graizer, K. Hudnut, C. Ji, L. Jones, J. Langbein, J. Lin, E. Roeloffs, R. Simpson, K. Stark, R. Stein and J.C. Tinsley, Preliminary report on the 22 December 2003, M 6.5 San Dimeon, California earthquake, *Seismol. Res. Lett.*, 75(2), 155-172, 2004.

Jennings, C.W., *Fault Map of California with Locations of Volcanoes, Thermal Springs, and Thermal Wells*, Geologic Data Map, California Division of Mines and Geology, no. 1, 1975.

Shearer, P.M., Global seismic event detection using a matched filter on long-period seismograms, *J. Geophys Res.*, **99**, 13,713–13,725, 1994.

Non-technical Summary

We are developing methods for automatically detecting and locating very early aftershocks of large earthquakes to researchers to quickly identify the mainshock rupture direction and improve the rapid calculation of strong ground-motion predictions.

Reports Published

none